MAXIMUM POWER POINT TRACKING IN PHOTOVOLTAIC SYSTEMS USING MODEL REFERENCE ADAPTIVE CONTROL

by

Qinhao Zhang

B.S., Shanghai Jiao Tong University, China, 2011

Submitted to the Graduate Faculty of

Swanson School of Engineering in partial fulfillment

of the requirements for the degree of

M.S. in Electrical Engineering

University of Pittsburgh

2012

UNIVERSITY OF PITTSBURGH

SWANSON SCHOOL OF ENGINEERING

This thesis was presented

by

Qinhao Zhang

It was defended on

November 19th, 2012

and approved by

Zhi-Hong Mao, Ph.D., Associate Professor, Department of Electrical and Computer Engineering

William Stanchina, Ph.D., Professor, Department of Electrical and Computer Engineering

Gregory Reed, Ph.D., Associate Professor, Department of Electrical and Computer Engineering

Thesis Advisor: Zhi-Hong Mao, Associate Professor, Electrical and Computer Engineering Department

Copyright © by Qinhao Zhang

2012

MAXIMUM POWER POINT TRACKING IN PHOTOVOLTAIC SYSTEMS USING MODEL REFERENCE ADAPTIVE CONTROL

Qinhao Zhang, M.S.

University of Pittsburgh, 2012

This thesis proposes adaptive control architecture for maximum power point tracking (MPPT) in photovoltaic systems. Photovoltaic systems provide promising ways to generate clean electric power. MPPT technologies have been used in photovoltaic systems to deliver the maximum power output to the load under changes of solar insolation and solar panel's temperature. To improve the performance of MPPT, this thesis proposes a two-layer adaptive control architecture that can effectively handle the uncertainties and perturbations in the photovoltaic systems and the environment. The first layer of control is ripple correlation control (RCC), and the second layer is model reference adaptive control (MRAC). By decoupling these two control algorithms, the control system achieves the maximum power point tracking with shorter time constants and overall system stability. To track the maximum power point as the solar insolation changes, the RCC algorithm computes the corresponding duty cycle, which serves as the input to the MRAC layer. Then the MRAC algorithm compensates the under-damped characteristics of the power conversion system: the original transfer function of the power conversion system has time-varying parameters, and its step response contains oscillatory transients that vanish slowly. Using the Lyapunov approach, an adaption law of the controller is derived for the MRAC system to eliminate the under-damped modes in power conversion.

Keywords: Photovoltaic system, maximum power point tracking, model reference adaptive control and ripple correlation control.

TABLE OF CONTENTS

LIST OF TABLES

LIST OF FIGURES

PREFACE

Firstly, I'd like to extend my sincere appreciation to my committee, my advisor Professor Mao for his guidance in my academic study and offering me the opportunity to participate in this exciting research, Professor Stanchina for his trust and valuable suggestions, and Professor Reed for his generous advice and support.

Secondly, I'd like to extend my thanks to senior graduate student, Raghav Khanna, who collaborated with me in this project and gave me helpful suggestions. In addition, with Raghav Khanna's kindly permission, I can use part of the research achievement written in another paper.

Finally, I'd like to thank my friends and family. They are always supportive and inspiring to my decision.

1.0 INTRODUCTION

1.1 BACKGROUND

Photovoltaic system is a critical component to achieve the solar energy through an environmentally-friendly and efficient way. Maximum power point tracking algorithm (MPPT) keeps the photovoltaic systems continuously delivering the maximum power output to the utility, regardless of the variation in environment condition. Under the effect of MPPT algorithm, the photovoltaic systems are capable of adapting itself to the environment change and delivering the maximum power output. Generally, the MPPT controller is embedded in the power electronic converter systems, so that the corresponding optimal duty cycle is updated to the photovoltaic power conversion system to generate the maximum power point output.

A series of the control algorithms for the MPPT are well understood at the present time, due to the significance of improving the photovoltaic systems performance efficiency. The underlying principle of maximum power point tracking algorithm is to use the ripple voltage or current component to identify the variation trend of the power output with the knowledge of the current versus voltage and the power output versus the voltage of the PV system. Generally, the operating point for different environment conditions varies and the characteristics of the *I*-*V* and *P*-*V* are generally illustrated in the way shown in Figure 1. The corresponding voltage array for the maximum power point is varied, as a result of the variation in the solar insolation and the panel temperatures. By implementing the

photovoltaic system with a DC-DC converter integrated with an MPPT controller, the nominal voltage can be modulated so that the maximum power is delivered. To track the maximum power point with dynamic changes, many algorithms deliver appropriate solutions in literature to solve the problem.

Many refined MPPT algorithms have been optimizing the digital realization, implementation complexity and operating cost since 1970s. Among these algorithms, ripple correlation control (RCC) is a better solution to solve the MPPT problem, considering the issue of stability, complexity and expense. Ripple correlation control is utilizing the integration of the correlation between the ripple power component and the ripple current or voltage component in the power electronic systems to obtain the duty cycle of the optimal power output.

The other control algorithm is model reference adaptive control (MRAC). It is designed to compensate for changing the undesired characteristic of the photovoltaic power conversion system. As a result, the performance of the power output is improved. MRAC has been analyzed since 1968 and has already been a widely-used technology in the modern control engineering and many other fields. MRAC is one of the robust prevalent control approaches in the adaptive control branch because MRAC is expertise in tuning the system's performance to the nominal characteristic when the system's parameter is unknown at prior.

In this project, under the effect of environment conditions, the specific dynamics of the power conversion system, or equivalently, the transfer function of the plant, is a nonlinear system. In each specific working environment, an equivalent transfer function between the duty cycle and the voltage array output can be uniquely determined. Therefore, the MRAC algorithm is a suitable solution to alter the characteristics of the plant, considering the unknown parameters of the single-input single-output plant (SISO). In the MRAC algorithm, given a nominal reference model for photovoltaic system, through constantly tuning the

parameters of the controller, the characteristics of the plant will converge to the characteristics of the reference model, meanwhile, the deviation between the reference model and plant model output will approach to zero, gradually.

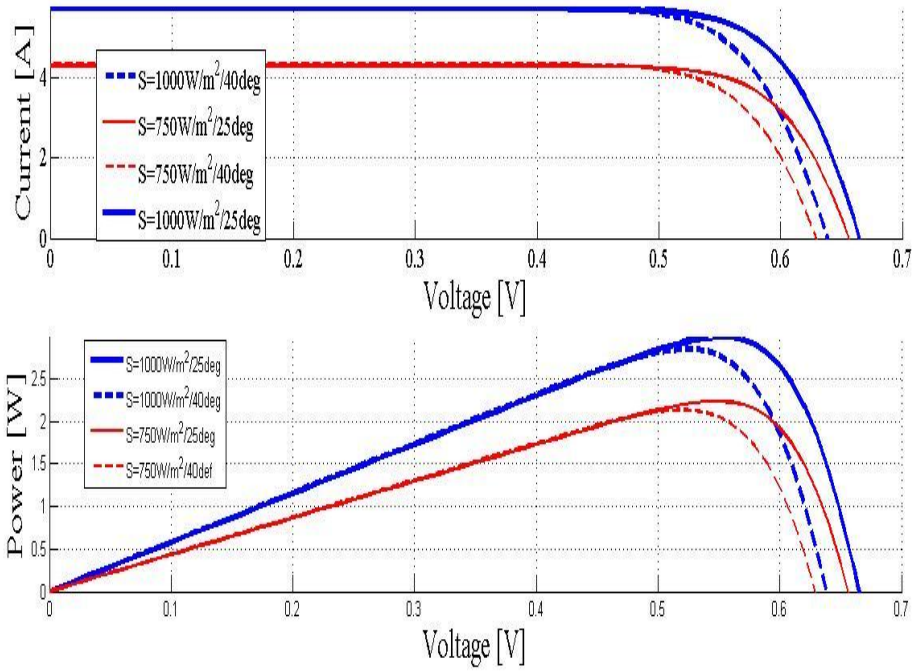

Figure 1: I-V and P-V curve for photovoltaic system with different irradiance and temperature.

1.2 MOTIVATION AND PROBLEM STATEMENT

As reported in the given literature, the dynamics of the power conversion system possesses an under-damped characteristic and the occurrence of oscillation in the transient period before converging to the nominal voltage output [1]. In term of MPPT, the voltage output array oscillates back and forth around the nominal voltage value, due to the under-damped characteristic of the photovoltaic system. Compared with an under-damped system, a

critically-damped system converges to the steady state within a shorter time and there is no oscillation in the transient period. Such result infers that the adapted system will optimize the voltage response if the MRAC design is used to draw the unknown characteristic of the plant model to the desired one.

This project proposes a control structure to optimize the performance of the maximum power point tracking, by coupling two distinct control algorithms together. The first layer of the system is ripple correlation control algorithm, as briefly introduced in background Section. The duty cycle for tracking maximum power point under different solar insolation is obtained within a short time. Then the duty cycle is input into the transistor in the power conversion system, and its transfer function describes the relationship between the change of the duty cycle and the change of the array voltage output. The second layer of the system is model reference adaptive control, which is used to improve the performance of the response trajectory. Due to the value of the electronic components in the circuit, the transfer function of the plant is always an unknown parameterized under-damped system and its step response shows decaying oscillation in the transient period. Under the effect of external condition changing, it is not feasible to direct tune the system by changing the system's parameters. Instead, the characteristic of the plant model will converge to the desired characteristic and the time of tracking maximum power point will be less through the MRAC algorithm,. In term of the curve of *P*-*V* characteristic, the optimized voltage output will display a straightforward trajectory to the maximum power point without oscillation.

These two control algorithms, as already shown in literature, are independently stable [2, 3]. However, it is not necessary to infer that the entire coupling system is stability. As a matter of fact, providing that these two control algorithm's time constant being significantly disparate, one can decouple these two algorithms so that the overall system is stable for certainty.

In this project, the main object is to design a robust model reference adaptive control to optimize the performance of maximum power point tracking in order to eliminate the oscillation during the transient period after the adaptation session. For the main content of this thesis report, it is primary about the designing procedure, the simulation test analysis and result discussion of the robust model reference adaptive control. In the future work, the ripple correlation control will get further improved. Yet, to maintain the integrity of the description for the entire control system structure, both detailed derivation and analysis of MRAC and RCC will be shown in the Section 3.

1.3 RESEARCH HYPOTHESIS

More than a hundred documents have well analyzed the improvement of the photovoltaic systems by solving the MPPT problem; however, quite few attentions have distributed to the MRAC algorithm. Since the actual external environment change is hard to model in the simulation, the issue of robustness and stability should be well-considered in the designing work. To demonstrate the hypothesis of stability and feasibility for entire proposed control structure, three research goals are set.

Firstly, the research object is to design an MRAC controller to change the unknown plant characteristic with asymptotically convergence condition. Secondly, by testing the MRAC designing with different simulation inputs, a valid proof the robustness of the control system will be established. Thirdly, briefly describing the entire flow of the control system structure to ensure the entire stability condition being satisfied and the specific implementation of the system, although, it is quite hard to actually implement the simulation on the solar panel.

This thesis report is the first step of the design for the entire MPPT control system. As briefly discussed before, in future, series of optimizing analysis will continuously developed to improve the overall control design. For the rest of this paper, Section 2 will describe the main structure of the control system. Section 3 will show the design procedure of MRAC and related educational background of designing issues. Section 4 will demonstrate the robustness and stability of the control design. Finally, the conclusion of this research is in Section 5.

1.4 LITERATURE REVIEW FOR RCC AND MRAC ALGORITHMS

Several prevalent methods of solving MPPT problem are widely used in the industry. One algorithm is called the perturb and observe MPPT method (P&O MPPT) [4]. This method utilizes the additional perturbance component in the voltage or current array to constantly check whether the system has achieved the nominal current or voltage value. If the voltage is changed due to a given direction perturbance and the power output increases simultaneous, it means the maximum power point will be obtained with further such perturbance for the voltage; on the other hand, if the power output decreases with the same voltage perturbance, it means the maximum power point can be found with a reversed-direction perturbance in the current or voltage. Although P&O MPPT algorithm is easy to implement at an inexpensive cost, this method constantly uses the oscillations to track the maximum power point even when the system is already in the steady state. The underlying factor is because P&O MPPT is hard to recognize the source of the perturbance during the system operating. Sometimes, the perturbance is due to the environment change and sometimes, it is due to the inherent generated perturbance. As the noise or perturbance always exists in the system, P&O system can never be stable at the nominal value.

The incremental conductance algorithm (INC) [1, 5] locates the maximum power point, according to the relationship between the power versus voltage, where the derivation of the power with the voltage is ideally equal to zero. Several literatures have reported its robustness performance, with the cost of hardware and software complexity. As a matter of fact, such condition is never exactly satisfied because of the noise, the measurement error and quantization errors. Meanwhile, INC algorithm also increases the computation time of MPPT algorithm.

Besides the P&O and the INC algorithms, there are many other advanced algorithms have been addressed, such as fuzzy logic and the neural network-based algorithms [6, 7]. These methods are suitable for solving certain specific problems; however, the realization of the system is overwhelmingly complex in the software and hardware construction of the solar panel. When the maximum power point is obtained, the correlation is equal to zero.

RCC method copes with many drawbacks of other algorithms [3, 8-10]. Several advantageous features of RCC, comparing to the other given methods have been discussed and generalized in literature [10]. Briefly, one factor is that RCC has a simple circuit implementation and fast computation time, compared to the incremental conductance (INC) method. INC method is also time-consuming in the simulation. Another factor is that RCC does not need intentional perturbance to generate the ripple component; instead, the perturbance already exists due to the switching converter in the circuit. Thirdly, the RCC system is asymptotically converging to the object and its converging rate can be tuned by the controller gain or the converter switching period. As the consideration of the complexity, cost, implementation factors, RCC algorithm is recommended to be used in this PV power conversion system application, although, there is no evident proof to suggest that there be a best solution in any MPPT problems.

Concerning about the method of MRAC, many literature reported the designing improvement and the specific implementation of MRAC [11-16]. MRAC is derived from the branch of the model reference control. In the MRC control, with the knowledge of the plant characteristic, the object is to generate the reference model to improve the performance of the system output. However, with the knowledge of the plant is unknown to the designer, MRAC is an alternative way to use the certainty equivalence approach to estimate the plant parameter. With the different methods used to estimate the plant parameters, different types of the MRAC will be classified. In this project, the strictly positive real-Lyapunov approach is preferable in finding the adaptive laws [14-16].

2.0 MAIN STRUCTURE OF ENTIRE SYSTEM

In the last section, the two-layer structure of the control system is briefly discussed, as shown in Figure 2. By mean of the MPPT controller, equivalently RCC algorithm, the duty cycle is fed into the switching transistor of the converter; hence the maximum power output can be found. Then through the MRAC component, the transfer function of the converter is adapted. After the adaptation, the maximum power output will be delivered to the utility.

In this project, it is required to obtain the model of the converter, as shown in Figure 2, which describes the relationship between the dynamics of duty cycle and the voltage output. When the duty cycle is updated, following by the environment change, the derivation of the voltage array in the solar panel will be updated as well. To get the transfer function of the actual plant, one can derive it through the equivalent small signal circuit of the photovoltaic power conversion system, as detailed shown in Figure 3 [17]:

As shown in Figure 3, the resistor R_{I} is analog to the solar irradiance or temperature change with the small signal of the voltage, $\tilde{v}_{\mathrm{PV}}$, to the small signal of the current, $\tilde{\imath}_{\mathrm{PV}}$. When the solar insolation changes, the specific operating point of the PV power conversion system changes, as a result, the value of the resistor varied. And hence the value of the resistor is unable to predict because it is extremely hard to predict the irradiance of the sun throughout a day. To obtain the characteristic of the nonlinear system, linearization at a certain operating point of solar intensity is required. And Figure 3 is the linearization process of the nonlinear system. As shown in the following, one can express the small signal equivalent circuit of the system in this way.

$$\frac{\tilde{v}_{\mathrm{PV}}}{R_{\mathrm{I}}} + s\tilde{v}_{\mathrm{PV}}C_{\mathrm{I}} = \frac{\dot{q}(D)\tilde{d} - \tilde{v}_{\mathrm{PV}}}{sL_{\mathrm{O}}} \quad \textbf{(2-1)}$$

where $\tilde{v}_{\mathrm{PV}}$ is the voltage input difference, corresponding to the solar insolation change. The resistor R_{I} is an equivalent representation of the current. The voltage over the booster converter is q(D), as a function of the DC component of the duty cycle, and the q(D) can be expressed as: q(D) = V_{PV} = (1-D) V_{O} $\rightarrow \dot{q}(D)$ = -V_{O}. If the relationship between the array voltage change to the duty cycle change is $G_{\mathrm{VP}}(s)$, then $G_{\mathrm{VP}}(s)$ can be expressed as follow:

$$G_{\mathrm{VP}}(s) = \frac{\tilde{v}_{\mathrm{PV}}}{\hat{d}} = \frac{\dot{q}(D)}{L_{\mathrm{O}}C_{\mathrm{I}}s^2 + \frac{L_{\mathrm{O}}}{R_{\mathrm{I}}}s + 1} \quad \textbf{(2-2)}$$

(2-2) can also be re-arranged into the following form and it is second order system:

$$G_{sec}(s) = \frac{\mu{\omega_{\mathrm{n}}}^2}{s^2 + 2\xi\omega_{\mathrm{n}}s + {\omega_{\mathrm{n}}}^2} \quad \textbf{(2-3)}$$

$$G_{\mathrm{VP}}(s) = \frac{\frac{-V_{\mathrm{O}}}{L_{\mathrm{O}}C_{\mathrm{I}}}}{s^2 + \frac{1}{C_{\mathrm{I}}R_{\mathrm{I}}}s + \frac{1}{L_{\mathrm{O}}C_{\mathrm{I}}}} \quad \textbf{(2-4)}$$

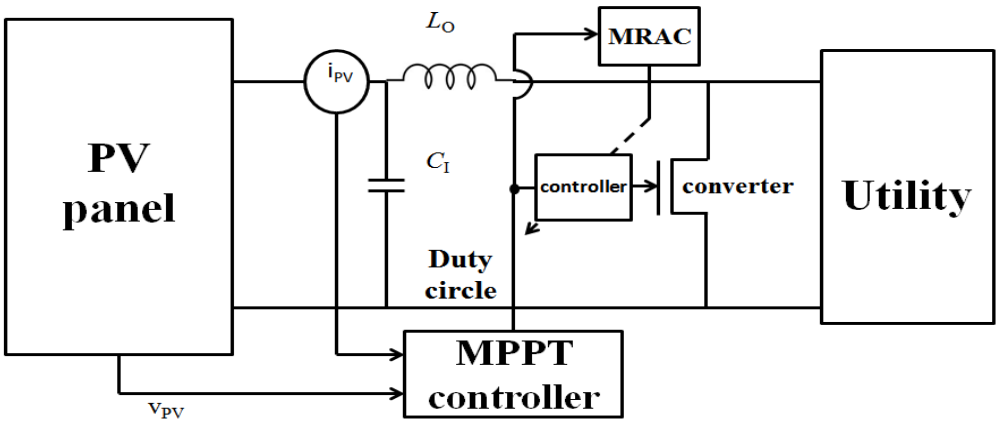

Figure 2: The scheme of entire control system.

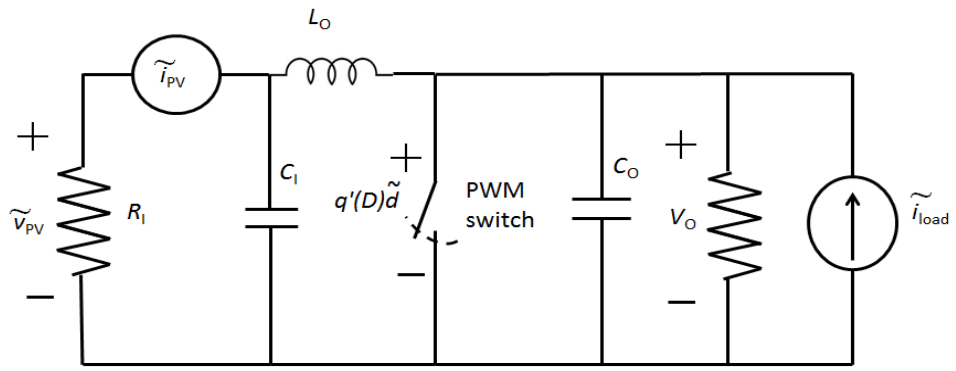

Figure 3: The equivalent small signal circuit of converter.

As seen in (2-4), this transfer function is derived from a linearization of a second non-linear system, seem in the Figure 3. The value of the capacitor and inductor are fixed. However, the external solar insolation changing constantly, as a result, different *P-V* curve would lead to the maximum power point at different region on that curve figures, which can be explicitly shown in the Figure 1. Similarly, varying environment condition will lead to varying value of the resistor, R_I, and it is hard to acquire the specific value of the resistor when the operating point of the system continuously changing. As a result, the damping ratio varies with the specific value of resistor and the step response of the voltage output with different equivalent value of resistor can be seen in the Figure 4:

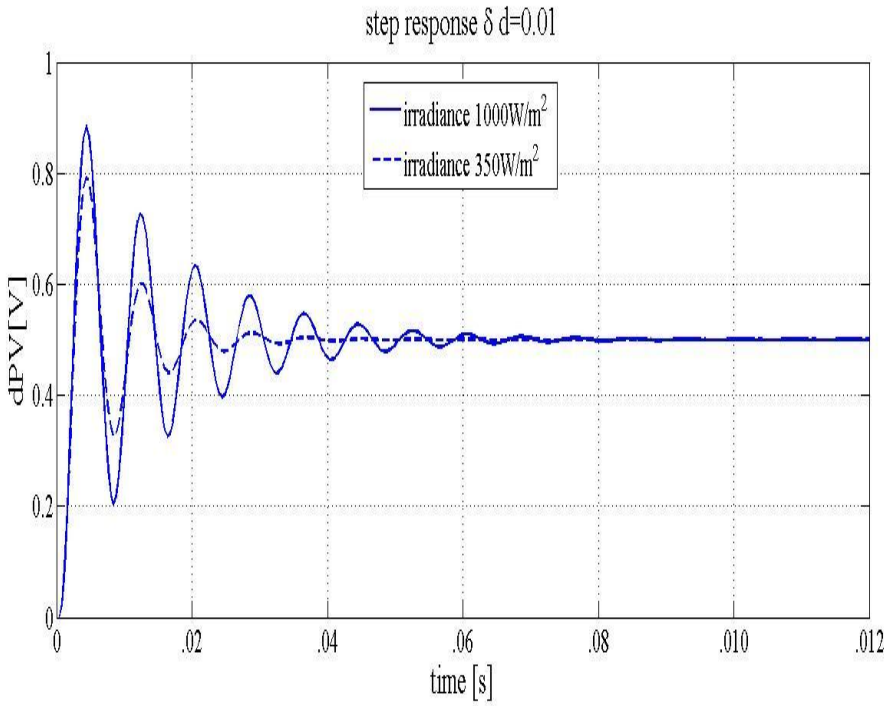

Figure 4: The step response of the under-damped converter.

In Figure 4, the voltage response shows the oscillation with different damping ratio and changing dc gain. With the effect of external irradiance change, such oscillation in the

transient period inevitable occurs and the various time constant for each distinct system which corresponds to the sunshine intensity, will significantly extend the converging rate of the converter and in the most time the system cannot deliver the maximum power output. Besides, there is no straightforward approach to estimate the parameters in the transfer function of the plant to change the characteristics of the plant and eliminate oscillation during the transient period. Therefore, it is necessary to use the mechanism of MRAC to solve the difficulty and improve the output performance of the system. Since the parameter of the transfer function, as shown in the (2-4), is changing swiftly, the Lyapunov-based direct MRAC algorithm is recommended to design a stable control structure to tune the plant. The related details and analysis will be extensively discussed as following.

3.0 DESIGN ANALYSIS FOR MRAC AND RCC

3.1 SCHEME OF THE MRAC AND PROOF OF STABILITY

As discussed in Section 2 that the transfer function between the duty cycle and the voltage output in the array is an under-damped second order system. When the updated duty cycle inputs into dynamic system, the voltage output will display decaying oscillation in the transient period and gradually converge to the nominal voltage of the maximum power point. It is desired that the transfer function has the critically-damped characteristic, not only because the time constant will be minimized compared to the time constant of the under-damped system, but also no oscillation will occur in the transient response. To obtain a critically damped response for the given transfer function, the general MRAC architecture is shown in the Figure 5.

The input to the overall system, r is the duty cycle obtained in the ripple correlation control method. The specific transfer function of the plant model, or equivalently the system of photovoltaic power conversion, can be obtained in the following section. Also, it is certainly that the transfer function of the plant model is a second order system and the relative degree of the system is two. The fundamental object of MRAC used in this project is to draw the characteristic of the plant to the characteristics of the reference model. By designing an ideal reference model, after adaptation, the plant model will have such characteristics as well. The result of each iterative comparison, between the plant and reference model output is the error signal. The error signal as well as the input and the output of the plant, adaptively

enable the adjustment parameters to tune the controller so that the parameters of the plant will converge to the parameters of the reference model. Eventually, the error between the plant and the reference model will drive to zero and the controller parameters will converge to the nominal controller parameters, so that the full convergence is achieved and thus the adapted array voltage tracks the theoretical MPP voltage. It is desired that the plant deliver a critically damped response under the essential condition that the input signal is persistently exciting.

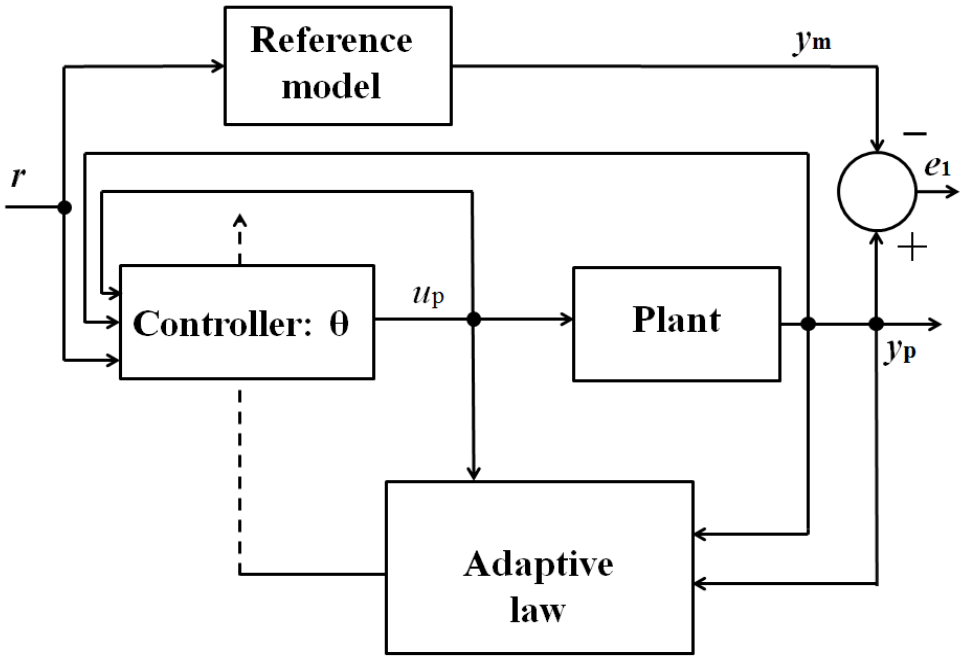

Figure 5: The general scheme of the MRAC structure.

Generally, for any signal, *u(t)*, is considered as persistently exciting if the following condition is satisfied:

$$\int_{t}^{t+T_0} u^2(\tau)d\tau \geq \alpha_0 T_0 \qquad \textbf{(3-1)}$$

in (3-1), for any positive value t, there exists α_0 and T_0 to meet the condition, then the signal *u(t)* satisfies the PE condition. It is also necessary to interpret that the input signal should be *2n* order with a given nth order plant model. In the simulation, it is instructive to know that the combination of step function and sin function are all satisfied with the PE condition.

In the general MRAC architecture, quite many different methods can be utilized to find the adaptive laws for the controller to make sure the error signal converge. Basically, the prevalent method at the present is using Lyapunov function to ensure the system converge asymptotically. There are several definitions to determine the meaning of stability in the control theory. The stability in the sense of Lyapunov is a mild approach to find the adaptive law by ensuring the asymptotic stability. An arbitrary point is stable if for any ϵ >0, there always exists a value δ >0, so that the norm value between the current point and the nominal equilibrium point is always less than the δ. In other word, the stability in the sense of Lyapunov is independent of the initial condition of the system and is significantly sufficient to guarantee the stability. As shown in Section 2, the relative degree plant of the photovoltaic power conversion system e.g. *(deg(D_{m})-deg(N_{m}))* is two. The transfer functions for the reference model is $G_{\mathrm{vm}}(s)$ and the plant model is $G_{\mathrm{vp}}(s)$, they can be represented as seen in (3-2):

$$G_{\mathrm{vm}}(s) = \frac{y_{\mathrm{m}}}{r} = k_{\mathrm{m}} \frac{1}{s^2 + a_{\mathrm{m}} s + b_{\mathrm{m}}} = k_{\mathrm{m}} \frac{N_{\mathrm{m}}(s)}{D_{\mathrm{m}}(s)}$$

$$G_{\mathrm{vp}}(s) = \frac{y_{\mathrm{p}}}{u_{\mathrm{p}}} = k_{\mathrm{p}} \frac{1}{s^2 + a_{\mathrm{p}} s + b_{\mathrm{p}}} = k_{\mathrm{p}} \frac{N_{\mathrm{p}}(s)}{D_{\mathrm{p}}(s)} \qquad \textbf{(3-2)}$$

where k_{m} and k_{p} are the chosen gain of the systems, and a_{m}, b_{m}, a_{p} and b_{p} are the chosen parameters of the reference model and the plant model. By tuning the parameters in

(3-2), a critical damping system can be obtained under the condition being satisfied: $a_{\mathrm{m}} = 2\sqrt{b_{\mathrm{m}}}$. Several assumptions about (3-2) should be announced before the further analysis:

• the numerator and the denominator of polynomial in (3-2) are monic Hurwitz.

• the reference model is controllable and observable.

• the relative degree of (3-2) are the same and it is known.

• the degree of denominator of plant and the sign of the gain, k_{p}, is known.

• both the reference model and the plant model are controllable and observable

The expression for the controller is the combination of the input, output of the plant and the input of the reference model, as seen in (3-3):

$$u_{\mathrm{p}} = \theta_1 \frac{\alpha(s)}{\Lambda(s)} u_{\mathrm{p}} + \theta_2 \frac{\alpha(s)}{\Lambda(s)} y_{\mathrm{p}} + \theta_3 y_{\mathrm{p}} + c_0 r = \vec{\theta}\vec{\omega} \tag{3-3}$$

In (3-3), u_{p} is the input to the plant, vector $\vec{\theta} = [\theta_1, \theta_2, \theta_3, c_0]$ is the parameter vector of the controller, which is updated through the adaptive law which is required to find. Furthermore, r and y_{p} are the input to the system and the output of the plant, respectively, while $\frac{\alpha(s)}{\Lambda(s)}$ is a arbitrarily designed *n*th ($deg(D_{\mathrm{m}})$-1) order stable filter as denoted in Figure 6. The filter is used to ensure the stability of the system through derivative operation in the high-order system. Actually, in the practical situations, the only available variables to be measured are the the input of the system, the output of the reference model and of the plant. Therefore, other forms of intermediate variables, such as high order differentiation of the output is hard to measure and the derivation operating will lead the system to be unstable and is unobservable. The polynomial $\Lambda(s)$ contains the polynomial $N_{\mathrm{m}}(s)$, the numerator of the transfer function for the reference model, and the expression of the polynomial is: $\Lambda(s) =$

$\Lambda_0(s)N_{\mathrm{m}}(s)$. In the state variable vector $\vec{\omega} = [\omega_1, \omega_2, y_{\mathrm{p}}, r]$, variable ω_1 is equal to $\frac{\alpha(s)}{\Lambda(s)}u_{\mathrm{p}}$ and variable ω_2 is equal to $\frac{\alpha(s)}{\Lambda(s)}y_{\mathrm{p}}$. To obtain the controller's parameter and converge the plant model to the reference model, one can substitute r for u_{p}, according to the relationship in (3-3). Then the transfer function between the input of the system, r and the output of the plant, y_{p}., can be obtained in (3-4):

$$\frac{y_{\mathrm{p}}}{r} = \frac{k_{\mathrm{p}}N_{\mathrm{p}}(s)\Lambda(s)c_0}{D_{\mathrm{p}}(s)\big(\Lambda(s) - \theta_1\alpha(s)\big) - \theta_2 k_{\mathrm{p}}N_{\mathrm{p}}(s)\alpha(s) - \theta_3\Lambda(s)k_{\mathrm{p}}N_{\mathrm{p}}(s)} \tag{3-4}$$

In the (3-4), there is one zero and three poles for the transfer function. Sometimes, it is hard to guarantee that the overall transfer function of the plant after the controller tuning still has the same order as previously, instead, some plant will be transformed into a new plant with the same relative degree and higher order. It is hard to recognize such changing by measuring those variables; nevertheless, it maybe jeopardizes the stability condition of the entire system. With those assumptions claimed before, it is ensured that there is one additional pole and zero cancellations in the overall system and the order and characteristic of the transfer function for the converter remain. Equating (3-4) to the transfer function of the reference model in (3-2), the characteristics of the plant will share the same characteristics of the reference model if the following conditions listed in (3-5) are satisfied:

$$\begin{cases} c_0 = \dfrac{k_{\mathrm{m}}}{k_{\mathrm{p}}} \\ D_{\mathrm{p}}(s)\big(\Lambda(s) - \theta_1\alpha(s)\big) - \theta_2 k_{\mathrm{p}}N_{\mathrm{p}}(s)\alpha(s) - \theta_3\Lambda(s)k_{\mathrm{p}}N_{\mathrm{p}}(s) \\ = N_{\mathrm{p}}(s)\Lambda_0(s)D_{\mathrm{m}}(s) \Rightarrow \dfrac{y_{\mathrm{p}}}{r} = \dfrac{y_{\mathrm{m}}}{r} \end{cases} \tag{3-5}$$

One crucial difficulty lying in this work is the unknown parameter of the power converter due to that changing resistor in the circuit, shown in Figure 3. Therefore, a reasonable approach to overcome the obstacle is using on-line estimation of the controller parameter to represent the nominal controller parameter. By using the adaptive observers to identify the parameters of the plant is documented in the literature. Since it is expected to use the SPR-Lyapunov method, the adaptive observer with the auxiliary input is recommended to guarantee that the controller parameter converges to the unknown values, which are the exact nominal parameters, as calculated in previous equations. Therefore, the entire control flow of the MRAC needs to be modified from Figure 5 into a new one as shown in follows, and it is reasonable to demonstrate the practical meaning of the controller expression in (3-3).

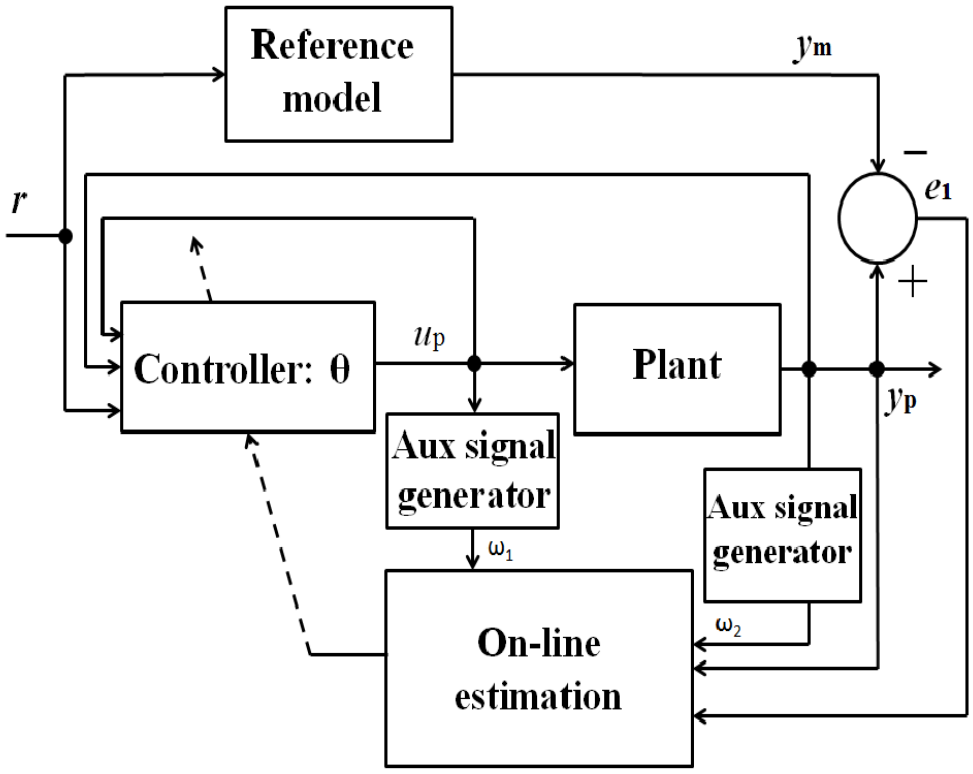

Figure 6: The proposed MRAC in MPPT.

As shown in Figure 6, the input and the output of the plant model are fed into the observer, so that the auxiliary signal ω_1 and ω_2 are joined into the on-line estimation to tuning the controller parameters. Therefore, several consequence need to be noticed: firstly, the parameter vector of the controller will be changed into the estimation parameter vector, $\overrightarrow{\theta^*}$. Secondly, with the realization of the adaptive observers in this system, the following properties can be guaranteed with the PE conditioned input:

• all the signals in the system are uniformly bounded

• the error between the actual output of the plant model and the estimated output of the plant model will approach to zero as time goes to infinity

• the error between the state space realization of the plant model and the estimated realization will converge to zero exponentially fast as time goes infinity.

By iteratively using the output of the reference model and the plant, the controller parameters converge to the nominal parameters. Thus, the form of u_p in (3-3) can be expressed as seen in (3-6):

$$u_\mathrm{p} = \overrightarrow{\theta^*}\overrightarrow{\omega} \tag{3-6}$$

Arbitrarily choosing $\Lambda(s) = 1 + s$ and hence $\omega_1 = \frac{\alpha(s)}{\Lambda(s)}u_\mathrm{p} = \frac{1}{1+\mathrm{s}}u_\mathrm{p}$ and $\omega_2 = \frac{\alpha(s)}{\Lambda(s)}y_\mathrm{p} = \frac{1}{1+\mathrm{s}}y_\mathrm{p}$. These two state observers equations can be represented as shown in (3-7):

$$\begin{cases}\dot{\omega}_1 = \omega_1 + u_\mathrm{p}, & \omega_1(0) = 0\\ \dot{\omega}_2 = \omega_2 + y_\mathrm{p}, & \omega_2(0) = 0\end{cases} \tag{3-7}$$

The observers in (3-7) are implemented to estimate the minimal realization of the plant to obtain the error between the reference model output and the plant model output [13]. The state-space realization of the transfer function for the plant and reference model, shown in (3-2), can be decomposed into the state space equation, shown as follows:

$$\begin{cases} G_{\mathrm{vm}}(s) = \dfrac{y_{\mathrm{m}}}{r} = C_{\mathrm{m}}(sI - A_{\mathrm{m}})^{-1}B_{\mathrm{m}} \text{ (reference model)} \\ G_{\mathrm{vp}}(s) = \dfrac{y_{\mathrm{p}}}{u_{\mathrm{p}}} = C_{\mathrm{p}}(sI - A_{\mathrm{p}})^{-1}B_{\mathrm{p}} \text{ (plant model)} \end{cases} \quad \textbf{(3-8)}$$

By substituting the input of the plant mode, u_{p}, with the controller expression, the state space of the plant model in (3-8) can be obtained:

$$\dot{x}_{\mathrm{p}} = A_{\mathrm{p}}x_{\mathrm{p}} + B_{\mathrm{p}}u_{\mathrm{p}}$$

$$\Rightarrow \begin{cases} x_{\mathrm{p}} = A_{\mathrm{p}}x_{\mathrm{p}} + B_{\mathrm{p}}(\theta^*{}_1\omega_1 + \theta^*{}_2\omega_2 + \theta^*{}_3C_{\mathrm{p}}x_{\mathrm{p}} + c^*{}_0r) \\ \dot{\omega}_1 = \omega_1 + \theta^*{}_1\omega_1 + \theta^*{}_2\omega_2 + \theta^*{}_3C_{\mathrm{p}}x_{\mathrm{p}} + c^*{}_0r \\ \dot{\omega}_2 = \omega_2 + C_{\mathrm{p}}x_{\mathrm{p}} \end{cases} \quad \textbf{(3-9)}$$

Since the object of the plant realization, shown in (3-9), is to be equal to the realization of the reference model under the factor of the controller, then the plant model, after the tuning, has owned the same state space realization as the realization of the reference model. Then the state-space equation for the overall closed-loop plant can be achieved by augmenting the state x_{p} of the plant with the states ω_1, ω_2 of the controller. Combining the controller expression in (3-3) with the observers equations in (3-7), the state-space equation model for the plant and reference model is obtained:

$$\begin{cases} \dot{X}_0 = A_1 X_0 + B_1 c^{0*} r + B_1 (u_\mathrm{p} - \theta^{*T} \omega) \\ y_\mathrm{p} = C_1^T X_0 \\ X_0 = \begin{bmatrix} X_\mathrm{p} \\ \omega_1 \\ \omega_2 \end{bmatrix} \\ A_1 = \begin{bmatrix} A_\mathrm{p} + \theta_3^* B_\mathrm{p} C_\mathrm{p}^T & B_\mathrm{p}\theta_1^* & \theta_2^{*T} B_\mathrm{p} \\ \theta_3^* C_\mathrm{p}^T & 1 + \theta_1^* & \theta_2^{*T} \\ C_\mathrm{p}^T & 0 & 1 \end{bmatrix} \\ B_1 = \begin{bmatrix} B_\mathrm{p} \\ 1 \\ 0 \end{bmatrix} \\ C_1 = \begin{bmatrix} C_\mathrm{p} \\ 0 \\ 0 \end{bmatrix}^T \quad (plant\ realization) \end{cases} \tag{3-10}$$

$$\begin{cases} \dot{X}_1 = A_1 X_1 + B_1 c^{0*} r \\ y_\mathrm{m} = C_1^T X_1 \\ X_1 = \begin{bmatrix} X_\mathrm{m} \\ \omega_{1\mathrm{m}} \\ \omega_{2\mathrm{m}} \end{bmatrix} \text{ (reference model realization)} \end{cases} \tag{3-11}$$

where $\omega_{1\mathrm{m}}$and $\omega_{2\mathrm{m}}$ are the observers for the reference model. The polynomial in the second equation of (3-5) is the determinant of matrix A_1. The roots of this polynomial are located in the left-hand side of the s-plane, according to the three roots, of the right hand side of the equation, are located in the left-hand side of the s-plane in (3-5). Therefore, it can be inferred that these two systems are stable. By subtracting the reference model's state space equation from the plant's state space equation, the state-space equations for the controller parameter's error and the tracking error are obtained as follows:

$$\begin{cases} \dot{e} = A_1 e + B_1 \left(u_\mathrm{p} - \dot{\theta^{*T}} \omega\right) = A_1 e + B_1 \tilde{\theta}^T \omega \\ e_1 = C_1^T e \end{cases} \tag{3-12}$$

where $e = X_0 - X_1$ is the state error, $e_1 = y_\mathrm{p} - y_\mathrm{m}$ is the tracking error signal of the plant, and $\widetilde{\theta}^T = \theta^T - \widetilde{\theta}^{T*}$ is the controller parameter's error between the nominal parameter and the actual parameter of the controller. The overall transfer function of the tracking error signal and the controller parameters error can be obtained as follows:

$$e_1 = C_1^T(sI - A_1)^{-1}B_1\widetilde{\theta}^T\omega = G_{\mathrm{vm}}(s)\frac{1}{c^{0*}}\widetilde{\theta}^T\omega \qquad \textbf{(3-13)}$$

Since matrix A_1 has proved to be stable, it is guaranteed that the tracking error will converge asymptotically with a bounded input signal and (3-13) is useful to find the adaptive laws for system with any relative degree. In finding the candidate of the Lyapunov-like function for (3-12), the equivalent transfer function of (3-13) should be a strictly positive real function (SPR function). The main reason of using Lyapunov-like function, instead of Lyapunov function, is because it is hard sometimes to find a Lyapunov function which is satisfied with the requirements for every system. Alternatively, by giving up several rigid requirements, Lyapunov-like function can also obtain adaptive laws for the stable convergence with sufficient condition.

In term of stability, a Lyapunov-like function is to obtain suitable adaptive law for the controller's expression. Applying an identity polynomial: $(s+g)(s+g)^{-1} = 1$ (term s+g needs to be stable) to both sides of (3-12) to decrease the relative degree of the overall transfer function, (3-14) is derived from (3-12):

$$\begin{cases} \dot{e} = A_1 e + B_1(s+g)\left(u_\mathrm{q} - \dot{\theta}^{*T}\phi\right) = A_1 e + B_1(s+g)\widetilde{\theta}^T\phi \\ e_1 = C_1^T e \end{cases} \qquad \textbf{(3-14)}$$

where several new state variables are introduced: $u_{\mathrm{q}} = \frac{1}{s+g} u_{\mathrm{p}}$, $\phi = \frac{1}{s+g}\omega = \frac{1}{s+g}[\omega_1, \omega_2, y_{\mathrm{p}}, r]^T$. The term $s+g$ will be absorbed into the matrix B_1. Since $u_{\mathrm{q}} = \theta^T \phi$, equivalently, the controller's input can be updated as:

$$u_{\mathrm{p}} = \theta^T \omega + \dot{\theta}^T \phi \tag{3-15}$$

The Lyapunov-like function has two error variables: the controller parameter error, $\widetilde{\theta}^T$, and the tracking error, e_1, based on the parameter estimation of the plant. Since the overall transfer function in (3-14) is strictly positive real function: $C_0^T(sI - A_1)^{-1}B_0 = (s+g)G_{\mathrm{vm}}(s)$, the corresponding Lyapunov-like function can be conventionally written as follows:

$$V(\tilde{\theta}, e_1) = \frac{e_1^T P e_1}{2} + \frac{\tilde{\theta}\Theta^{-1}\tilde{\theta}}{2} \left| \frac{k_{\mathrm{p}}}{k_{\mathrm{m}}} \right| \tag{3-16}$$

where *P* and Θ are two arbitrary selected positive definite matrices. Actually, Θ is the adaptive law gain matrix. It is a diagonal matrix; the larger value of the entries on the main diagonal, the faster convergence can be accomplished in the adaptation. The essential relationship between the condition of SPR and finding the existence of a Lyapunov function for a certain state space equation is according to the Meyer Kalman-Yakubovich (MKY) lemma.

According to the MKY lemma, given a stable strictly positive real transfer function for a system, *G(s)*, its minimum realization of the state space equation is the matrix *A*, vector *B* and *C* and scalar d (in this project, scalar is coincident zero for the plant model). Then for any symmetric positive definite matrix, *L*, there exists a positive vector *v* and a positive definite matrix *P*, such that the following equations for this project are satisfied:

$$\begin{cases} PA + A^T P = -qq^T - vL \\ PB = C \end{cases} \quad \textbf{(3-17)}$$

Based on the knowledge of MKY lemma, the derivation of the Lyapunov-like function seen in (3-16) along the solution of (3-14) is expressed as:

$$\dot{V}(\tilde{\theta}, e_1) = -\frac{1}{2} e_1^T qq^T e_1 - \frac{v}{2} e_1^T L e_1 - e_1^T P B_0 \frac{1}{c_o} \tilde{\theta}^T \omega + \tilde{\theta}^T \Theta^{-1} \dot{\tilde{\theta}} | \frac{k_\mathrm{p}}{k_\mathrm{m}} | \quad \textbf{(3-18)}$$

According to the definition of the stability in sense of Lyapunov stability, if the differentiation of the function $V(\tilde{\theta}, e_1)$ is less then zero, then the system is uniformly asymptotically stable. As seen in the (3-18, to find the adaptive law for the error of the controller parameter, it is suggested that the polynomial $-e_1^T P B_0 \frac{1}{c_o} \tilde{\theta}^T \omega + \tilde{\theta}^T \Theta^{-1} \dot{\tilde{\theta}} | \frac{k_\mathrm{p}}{k_\mathrm{m}} |$ be equal to zero will result (3-18 less than zero because of the polynomial: $-\frac{1}{2} e_1^T qq^T e_1 - \frac{v}{2} e_1^T L e_1$ less than zero. The system's output error and the controller parameter error are guaranteed to converge asymptotically to zero based on the controller parameter's updated law, as shown in (3-19):

$$\dot{\theta} = \dot{\tilde{\theta}} = \Theta e_1 \phi | \frac{k_\mathrm{p}}{k_\mathrm{m}} | \quad \textbf{(3-19)}$$

$$\phi = \frac{1}{1+s} \begin{bmatrix} (sI-1)^{-1} u_\mathrm{p} \\ (sI-1)^{-1} y_\mathrm{p} \\ y_\mathrm{p} \\ r \end{bmatrix}$$

Since the matrix A_1 is stable and the equivalent transfer function of the error of the output and the controller parameter, shown in (3-14) is strictly positive real function, it can be inferred that the error of the system output and the parameter error of the controller will converge asymptotically to zero, with the bounded source of the input, system output error and the choice of state variable vector. According to the derivations above, the overall

MRAC adaptive rules can be concluded as follows and each item in (3-20) is the function with zero value initial conditions:

$$\begin{cases} \dot{\omega}_1 = \omega_1 + u_{\mathrm{p}} \\ \dot{\omega}_2 = \omega_2 + y_{\mathrm{p}} \\ \dot{\phi} = -g\phi + \omega \\ u_{\mathrm{p}} = \theta^T \omega + \dot{\theta}^T \phi \\ \dot{\theta} = \Theta e_1 \phi |\frac{k_{\mathrm{p}}}{k_{\mathrm{m}}}| \end{cases} \quad \textbf{(3-20)}$$

A series of adaptive control updating laws are obtained in (3-20). With the entire scheme of MRAC found, two important conceptions are instructive to be informed: firstly, signal in the closed-loop plant is bounded and the tracking error signal will converge to zero asymptotically. Secondly, if the numerator and the denominator of the plant is coprime and the input signal is sufficiently rich of order, the tracking error signal will converge exponentially fast.

3.2 RIPPLE CORRELATION CONTROL

To deliver the maximum power output to the load at the steady state, RCC algorithm is utilized to calculate the duty cycle. RCC algorithm was recently developed and reported in [2, 3, 9, 18], where it was shown that the switching transistor will result in an inherent ripple voltage or current component, which can be utilized to track the location of the maximum power point. As briefly introduced in the Section 1.1, RCC algorithm is an improved algorithm based on the P&O method, because it avoids external energy to generate the

voltage ripple for tracking the MPP. In additional, it is proven in the report that RCC algorithm is asymptotically convergence to the MPP. As shown in the Figure 1, there is only one peak power value in the PV curve or the PI curve, where the maximum power delivery is obtained. Correlating the derivation of the power output and the derivation of the voltage output, the correlation identifies whether the present voltage is lower or higher than the nominal voltage output. To mitigate the array capacitance in the circuit, it is desired to use the ripple voltage component in the correlation, as the following formula to calculate the duty cycle shown:

$$\begin{cases} \tilde{p}_{\mathrm{PV}}\tilde{v}_{\mathrm{PV}} > 0 \ \text{ when } V_{\mathrm{PV}} < V_L^* \\ \tilde{p}_{\mathrm{PV}}\tilde{v}_{\mathrm{PV}} < 0 \ \text{ when } V_{\mathrm{PV}} < V_L^* \\ \tilde{p}_{\mathrm{PV}}\tilde{v}_{\mathrm{PV}} = 0 \ \text{ when } V_{\mathrm{PV}} = V_L^* \end{cases} \quad \textbf{(3-21)}$$

The control law can be seen in (3-22), as:

$$d = k \int \tilde{p}_{\mathrm{PV}}\tilde{v}_{\mathrm{PV}}\, dt \quad \textbf{(3-22)}$$

where $\tilde{p}_{\mathrm{PV}}$ and $\tilde{v}_{\mathrm{PV}}$ are the ripple component of the array power and voltage, and k is the negative valued gain. (3-22) can be described as follows: if v_{PV} increases and it result an increasing p_{PV}, the system's operating point is located on the left side of the MPP, therefore the value of d is decreasing; similarly, if v_{PV} increases and it result a decreasing p_{PV}, the system's operating point is located on the right side of the MPP. Inspecting (3-21) and (3-22), the maximum power point can be obtained when the derivation of d is equal to zero because that is the place where the voltage array is equal to the nominal one and the change of d can be assumed to zero. Given the mathematically proof for the stability of the RCC algorithm, the corresponding duty cycle for the maximum power point under various solar insolations

can be achieved. In the RCC algorithm, the underlying principle is using whatever ripple is already presented in the system to determine the location of the maximum power point.

Alternatively, the control algorithm by mean of the ripple current component can be realized as well because the *P-I* curve and *P-V* curve are similar to each other. One modification is the sign of the gain value of k needs to be reversed. However, due to the practical implementation, the issue of the parasite capacitor is necessary to be considered, the voltage ripple component is obviously advantageous than the current ripple component. As inferred from the literature review in Section 1, many improved and alternative version of RCC algorithms have been developed to replace the original one, another way to propose the RCC algorithm is using the direct integrand of the ratio between the power output and the ripple component of the voltage or the power output and the ripple component of the current:

$$d = \int \frac{dp}{dv_{\mathrm{L}}} dt \tag{3-23}$$

the control law in (3-23) is hard to expect working due to the complexity of realizing the integrand of this ratio in the circuit. Moreover, like the drawback of P&O MPPT algorithm, the ratio of signal-to-noise is unavailable and hence the (3-23) is not sufficient to make the judgment that the duty cycle for the maximum power point is achieved because the ratio between the ripple power and voltage component is impossible to maintain ideally being zero for quite amount of time. Due to the effect of noise, this control law is not reliable to make the determination.

With increasing focus on the simple implementation of the algorithm in circuit, one useful control law makes use of the sign function to track the MPP in the circuit. As shown the control law is:

$$d = k \int sgn(\frac{di_L}{dt}) sgn(\frac{dp}{dt})\, dt \quad \textbf{(3-24)}$$

the effect of noise is mitigated because of the sign function only focus on whether the derivation of d is larger, smaller or equal to zero. And this control law is easy to realize in electronics hardware by using logic circuit at an inexpensive cost. This control law was also proved mathematically that it is stable, and thus it is an alternative RCC algorithm to be used in this project.

4.0 RESULTS AND DISCUSSIONS

It is recommended to notice that when two distinct control algorithms decoupling together, it is not necessary to infer that the overall system is stable. However, as reported in the literature and analysis, the time constant of the two control methods are significantly disparate: RCC is several milliseconds and the MRAC is several seconds. Thus, when decoupling these two control algorithms together, the overall system will be stable for sure.

4.1 SIMULATION SETUP

In the project simulation, based on the given literature, the duty cycle is easily obtained and to be the input of the following MRAC system. The input of the system is modeled as two types signal function: one is the step function and the combination of step function, where the first one can be analog to the abrupt change of sunshine strength or the solar panel's temperature drop or jump in the practical situation and the latter one can be used to simulate the digital output of the RCC with short sample rate; the other type is the combination of several sine wave functions, which is generally analog to the smooth changing of the external environment changing in the most cases. These two types of input test the system from the view of magnitude and frequency characteristic. And the inputs are satisfied with the condition of persistence exciting.

Analytically, when the characteristics of the plant and the reference model are explicitly known as in the format of (3-2), the nominal controller parameter vector, $\vec{\theta}$ can be easily obtained, through equating (3-2) to (3-6) and choosing a stable filter $\Lambda(s) = \frac{1}{s+a}$(variable a is any positive real number). The nominal parameters of the controller are seen in (3-21):

$$\begin{cases} c_0 = \dfrac{k_\mathrm{p}}{k_\mathrm{m}} \\ \theta_1 = a_\mathrm{p} - a_\mathrm{m} \\ \theta_2 = \dfrac{(a_\mathrm{p} - a_\mathrm{m})(-a^2 + aa_\mathrm{p} - b_\mathrm{p})}{k_\mathrm{p}} \\ \theta_3 = \dfrac{(b_\mathrm{p} - b_\mathrm{m}) + (a_\mathrm{p} - a_\mathrm{m})(a - a_\mathrm{p})}{k_\mathrm{p}} \end{cases} \quad \textbf{(4-1)}$$

Providing the knowledge of these parameters, it is easy for the designer to see whether the MRAC structure works in the expecting scenario that the estimated controller parameter converges to the nominal parameters of the controller obtained in (4-1). This design could be realized in circuit, nevertheless, the simulation is set up in *Simulink* and the simulation time is approximately normalized into the actual time.

In the simulation, the reference model is designed to be a critically-damped second-order system and the plant is an under-damped second-order system. In selecting the parameters for the critically damped reference model, the damping ratio of $\frac{a_\mathrm{m}}{2\sqrt{b_\mathrm{m}}}$ is the determining factor as inferred in (3-2). Normally, the damping ratio for the critical damped system is chosen to be either exact one or slightly less than one, because the system's converge rate will be improved at the cost of slightly overshoot in the transient period of the output response. Secondly, the natural frequency of the plant is fixed by the selection of the capacitor and the inductor in Figure 3, which can be expressed as: $\sqrt{\frac{1}{L_O C_\mathrm{I}}}$. From the view of

energy saving and fast convergence, the natural frequency of the reference model is suggested to be close to the natural frequency of the plant model. Thirdly, to make the algorithm easy to implement, the dc gain of the reference model is suggested to design equally to the dc gain of the plant model. So that the system will not require extra control method to make the system responses of the reference model and plant model have the exact same curve shape. Upon these considerations, the parameters of the reference model are selected as following.

To overly test the performance of the MRAC controller design, two plant models are arbitrarily designed. As seen in Table 1, the damping ratio for the plant model II is much smaller than the damping ratio for the plant model I, as a result, the characteristic of plant model I is different from the characteristic of plant model II. As shown in Figure 7, the plant model II converges to the nominal voltage output swiftly and the envelop of the oscillation in plant model I decays slowly. By tuning these two plant models with significantly characteristic differences, the conclusion of the designed MRAC performance is adequate for the validity.

Table 1: Parameters for the simulation

Parameter	Reference model	Plant model I test	Plant model II test
k_0	9	9	9
a_0	6	0.2	0.006
b_0	9	9	9
a	1	1	1
damping ratio	1	0.0333	0.001

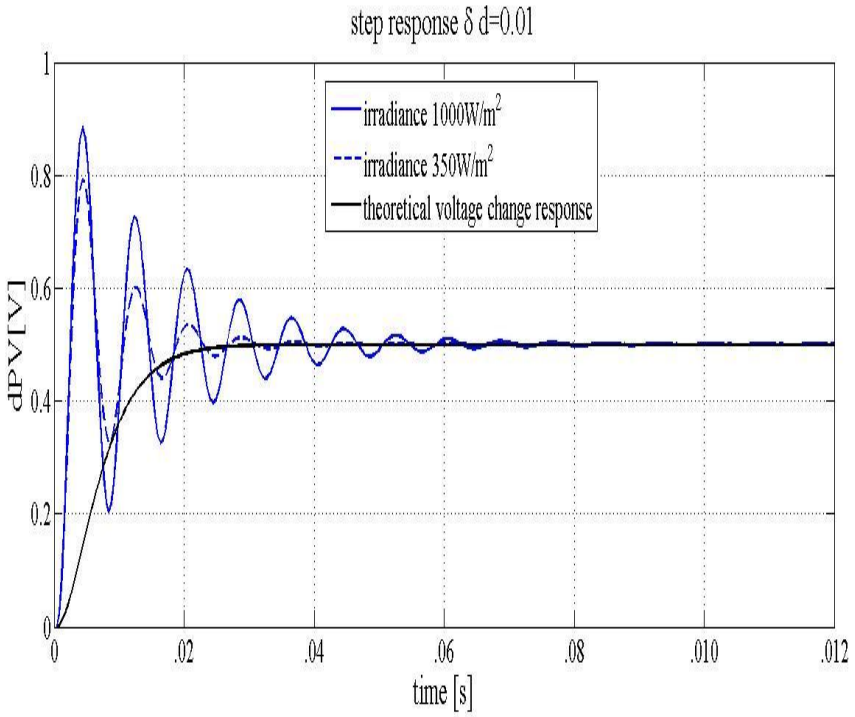

Figure 7: The step response of the converter.

4.2 STEP RESPONSE OF THE SYSTEM

The input signal to the system should have rich frequency components so that the output of the system carries sufficient information of the system and also guarantee the convergence. In this simulation, the input signal is designed to be a pulse width modulated (PWM) signal. In each periodic step change sequence, the tracking error and the controller parameter error are calculated to update the controller's parameters and converge the characteristics of the plant to the reference model's.

In Figure 8, it shows an explicit comparison in the early stage of the adaptive session for plant model I, while in Figure 9, it shows the adaptation information in the early stage of the plant model II. In each figure, there is a distinct difference between the step responses of the reference model, the plant with MRAC and the plant without MRAC. The period of the

pulsed modulated width signal is 1.2 seconds. In the first 0.6 second, the voltage output without using MRAC displays decaying oscillation and gradually converges to the nominal voltage value in approximate 0.3 second. On the other, in the initial stage, under the effect of the controller, there are significant oscillates for the system using MRAC in the voltage output and it illustrates the maximum derivation, which is even larger than the derivation between the output of the plant model without using MRAC and the output of the reference model. The maximum derivation between the plant model using MRAC and the reference model occurs after around 0.03 second. After that, the oscillation of the step response for the adapted plant converges to the steady state for another 0.06 second. It seems that the plant has been tuned to acquire similar characteristic of the step response for the reference model and the time duration of such adaptation is very short, and this time constant is even shorter than the time constant of the plant model without using MRAC. As illustrated in the next half period where the state changing from one back to zero, the voltage output approaches to steady state without any oscillations and the approaching curve is close to the curve of the reference model's response.

By comparing Figure 8 and Figure 9, it is surprisingly to find that the initial adaptation process for two plant model is quite similar to each other. With the same control structure of MRAC, the convergence of the characteristic of plant model is exponentially fast.

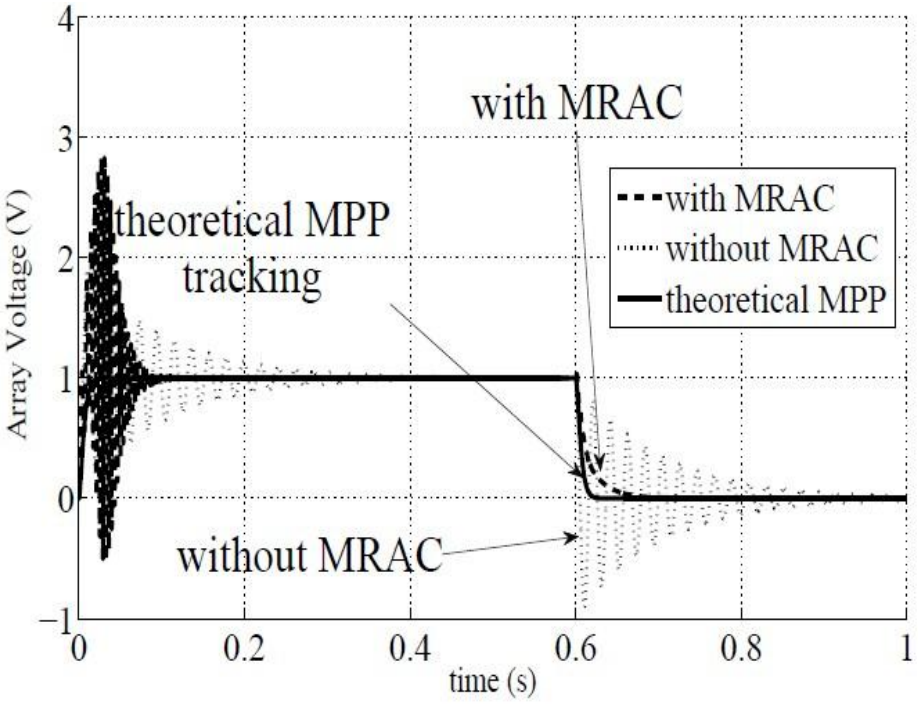

Figure 8: The step response comparison of plant model I in initial stage.

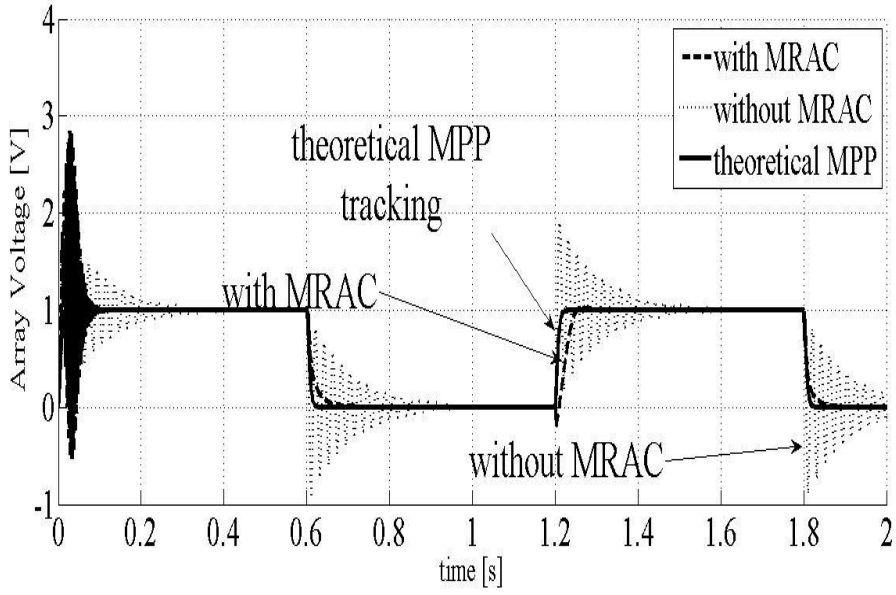

Figure 9: The step response comparison of plant model II in initial stage.

In the Figure 10, one feature of this figure is that the voltage response of the system without using MRAC has positive feedback after each period. The period of the PWM signal in Figure 10 is changed from the one-third of the original period. Since in the real application, the duty cycle will constantly feed into the system of converter, which means there is no sufficient time for the system to adapt the characteristic of the reference model, according to each step response. Under the condition that the plant model has a very low damping ratio, the original plant model is vulnerable to the small-period PWM input, which satisfied the PE condition. As shown in the figure, the oscillation range of the system without using MRAC increases with each toggle state of the PWM input. However, as an explicit comparison, under the effect of the MRAC controller, not only the plant model has not been affected by the harsh condition of the input, but also the voltage response of the system using MRAC has similar response trajectory after couple periods.

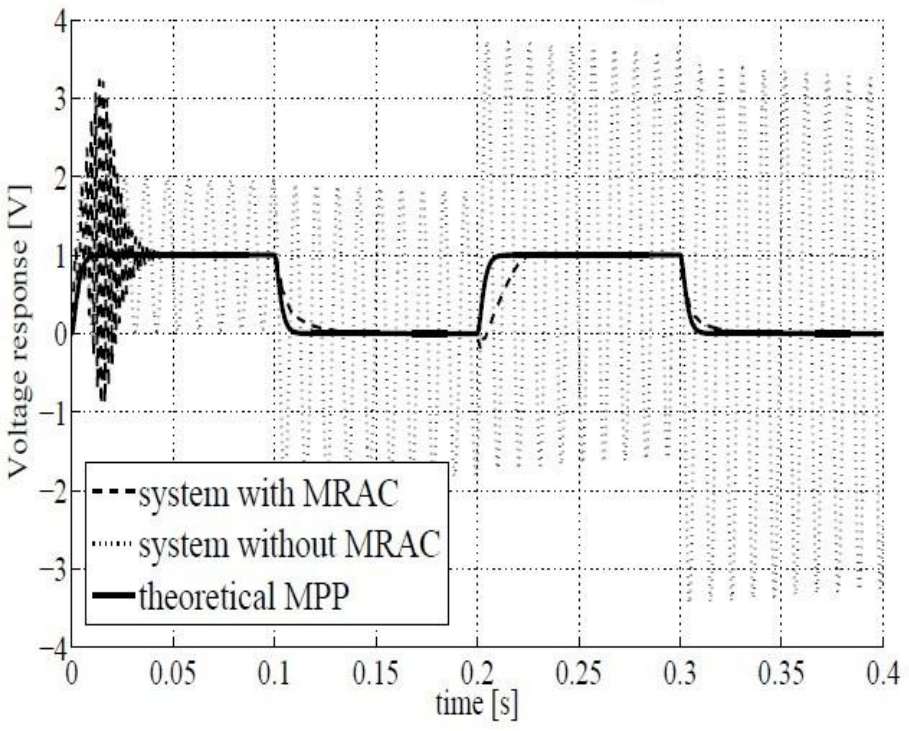

Figure 10: The step response of plant model II in the initial stage with different PWM input.

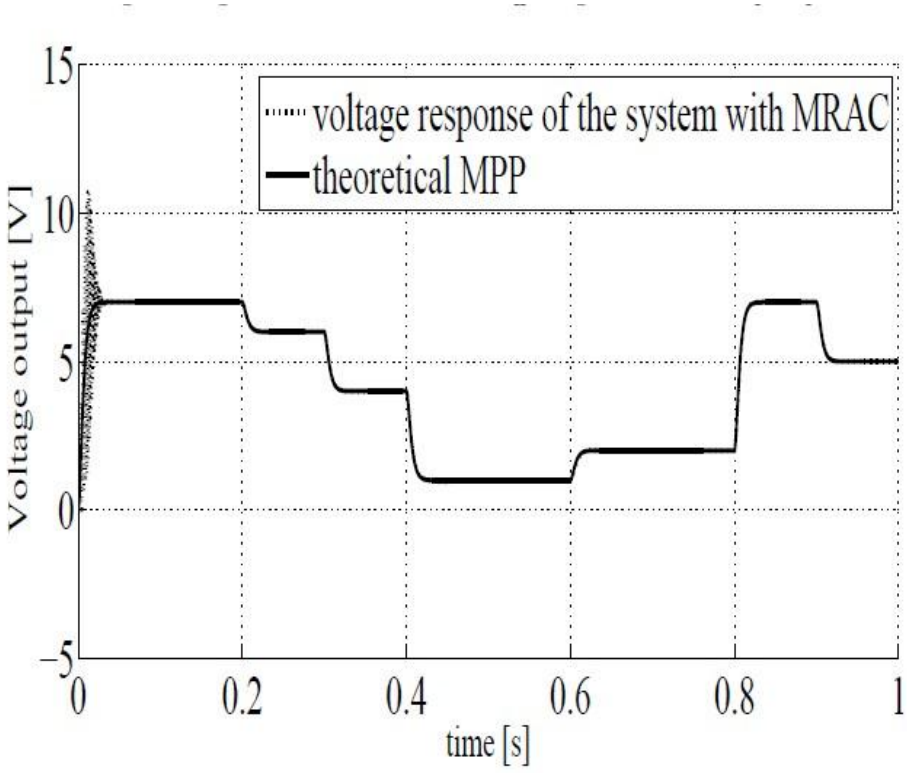

Figure 11: The step response of plant model I with the input signal analog to the duty cycle.

In the Figure 11, the input is designed to be the combination of PWM signal inputs with different magnitudes and periods. This input is very analog to the duty cycle obtained through the RCC algorithm in the real experiment. Due to the fast convergence in the RCC and the existence of sample rate in the electronic circuit, the amplitude of the input to the power converter is varying within a certain range and the changing interval is very short, such as 0.1 second as shown in the Figure 11. To demonstrate the robustness of MRAC controller design, it is clearly shown in the figure that the adaptation session only occurs in the very first moment, approximately lasting for 0.02 second. By tuning the adaptive gain matrix, which is mentioned in previous Section, the rate of convergence could be modulated, according to different requirement.

In the Figure 12, after 3 seconds adaptation, the voltage response of the adapted plant is very close to the response of the reference model, while the un-adapted plant still displays large magnitude and time-duration oscillation in each transient period. By using the PWM signal as an input, it is explicit to find the adaptation process of the plant model in each iteration step function. The controller parameter is constantly tuning that with the same step function input, the error between the reference model and plant model is converging to zero. As seen in Figure 12, the error between the step response of the adapted plant and the reference model is almost negligible and the only distinct error is in the very first time that the duty cycle switches between state one and state zero abruptly. Considering the very short time duration of such error and small magnitude, the error signal is negligible as well. Therefore, it is true that adapted plant has almost converged to the reference model in the sense of magnitude characteristic.

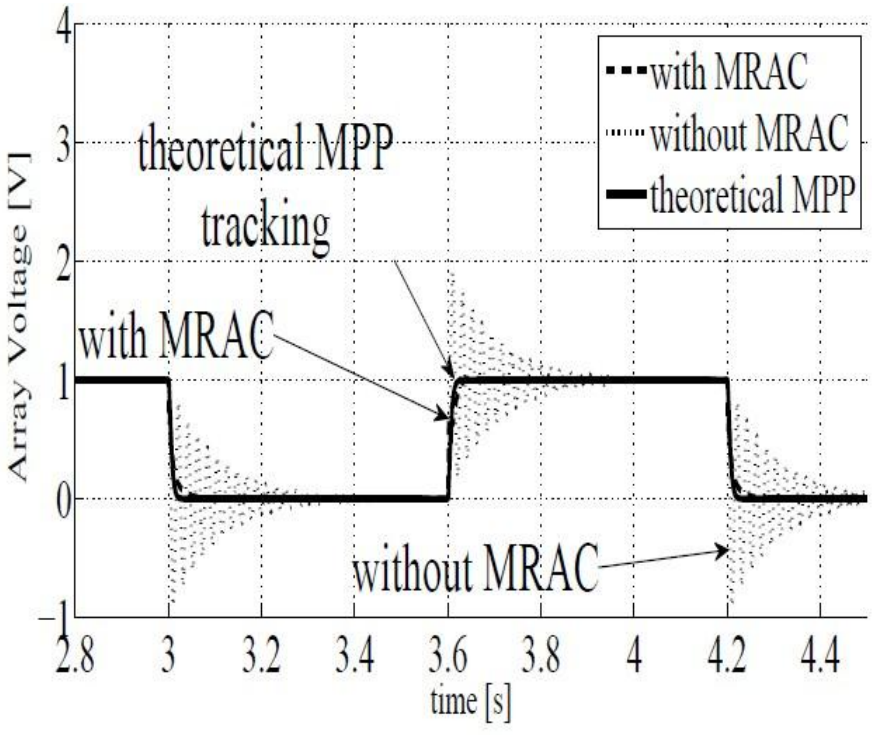

Figure 12: The step response comparison of plant model I after the adaptation stage.

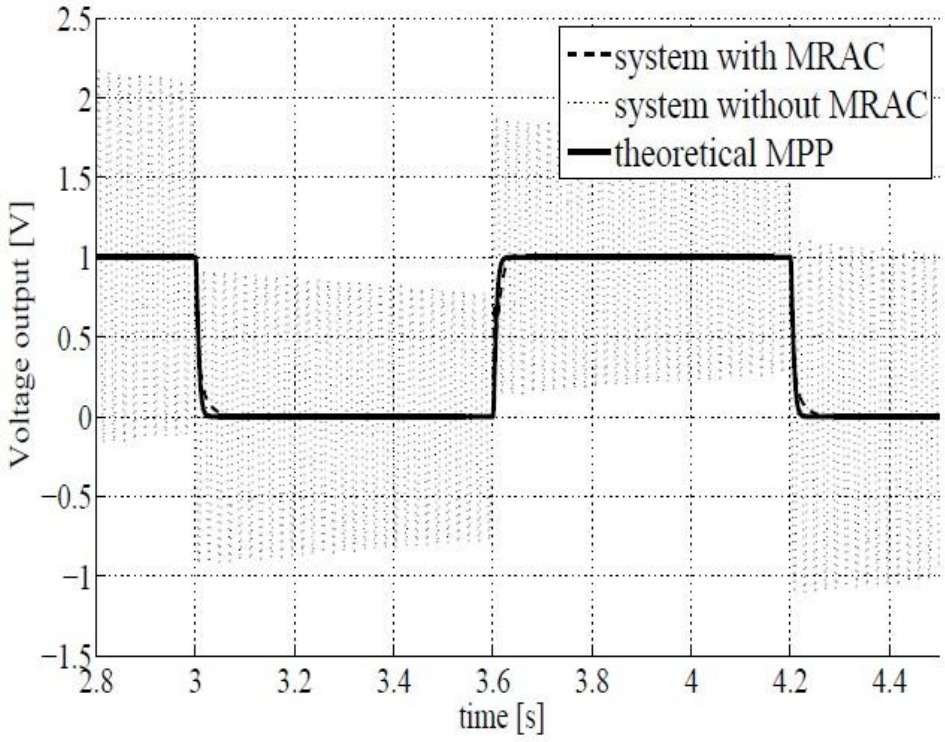

Figure 13: The step response comparison of plant model II after the adaptation stage.

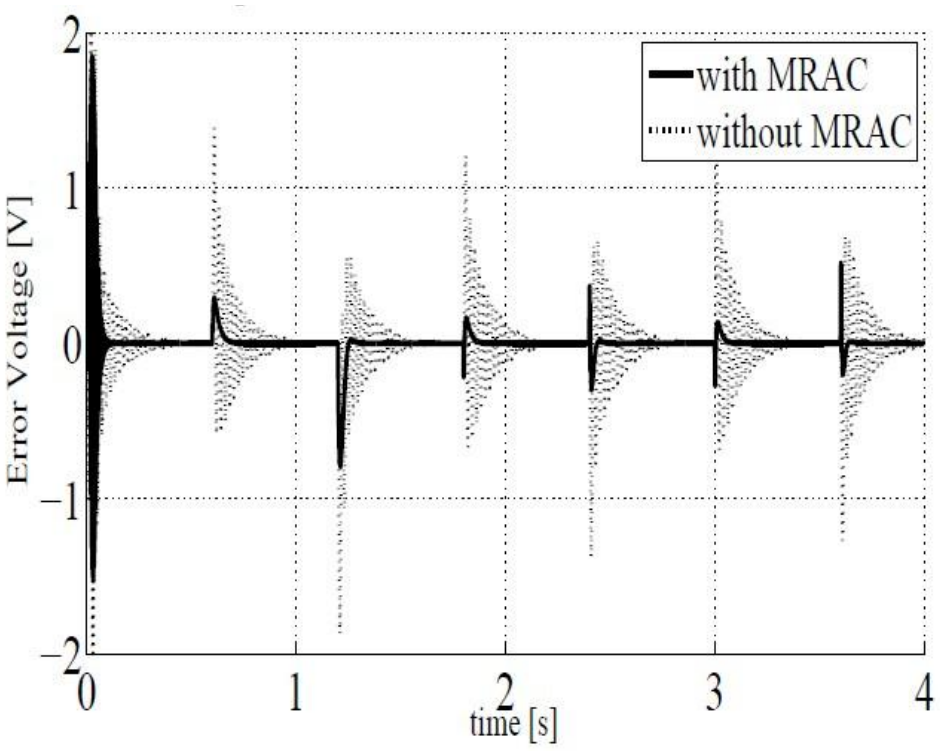

Figure 14: The error signal comparison for plant model I.

In Figure 14, it shows the tracking error over the time. One is the error between the output of the plant with MRAC and the reference model; the other one is the error between the output of the plant without using MRAC and the reference model. As seen in Figure 14, in the first stage, the thick line error signal is significant because of the adaptation process. However, as the plant continues to learn during the adaptive session, after 0.1 seconds, the error signal converges into a much smaller range and ultimately converges to zero. For each 0.6 second, the error signal strike for a very short time due to the abrupt change at each step, and then remain zero afterward. As time goes, the error strike decreases in magnitude and time duration.

4.3 RESPONSE OF THE SYSTEM USING SINE WAVE INPUT

Figure 15, Figure 16 and Figure 17 are the set of comparisons of the plant model using the sine wave function. In Figure 15 and Figure 16, one signal is the theoretical voltage output with the reference model; the other two are the outputs from the system using MRAC and without using MRAC. The input of the simulation consists of three frequency components. The output response of the system at the steady state will display stable frequency components, namely, each period will highlight the frequency characteristic. As shown in Figure 15, the output response of the system using MRAC obtains the frequency characteristic of the reference model after the first period. However, the output response of the system, without using MRAC, shows disparate frequency characteristic. By comparing the Figure 15 and Figure 16, it is shown that the system with using MRAC has a quite similar response curve shape and has a shorter time constant to convergence to the frequency steady

state of the reference model. While, the output responses of the system without using MRAC show different curve due to the difference in the plant model I and II. Also, as shown in the Figure 17, the error between the reference model and system using MRAC is almost zero after the initial adaptation session. According to these two types of input to the MRAC structure, the voltage output of the system using MRAC converges stably to the reference model in short time-duration. Such result well demonstrates the stability and robustness of realization for the MRAC design.

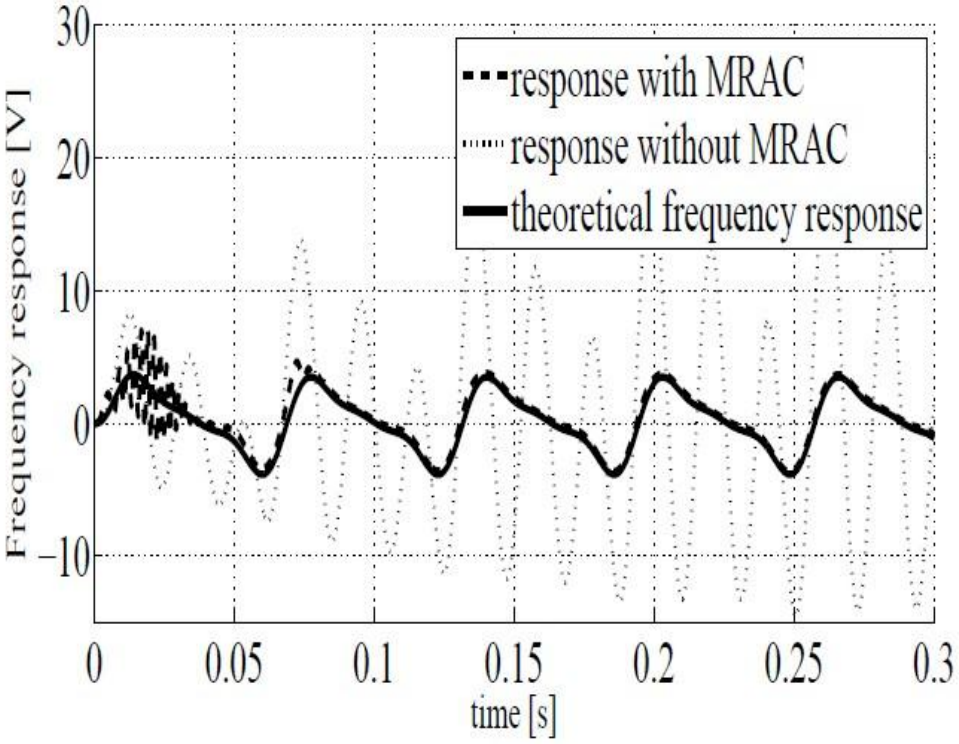

Figure 15: The response of plant I in the initial stage.

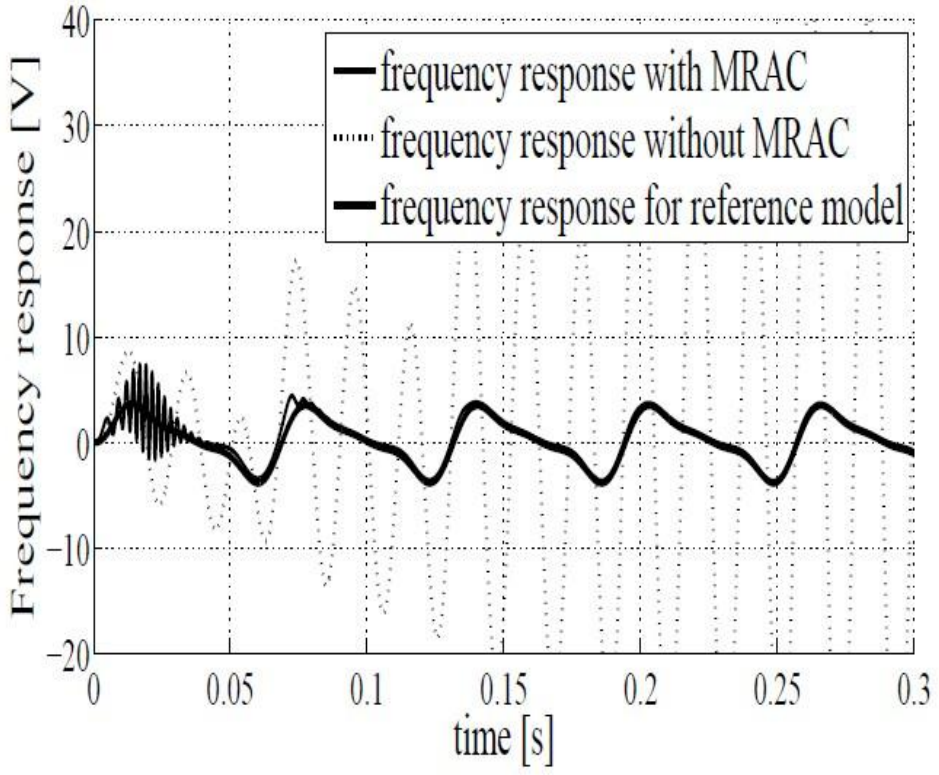

Figure 16: The response of plant II in the initial stage.

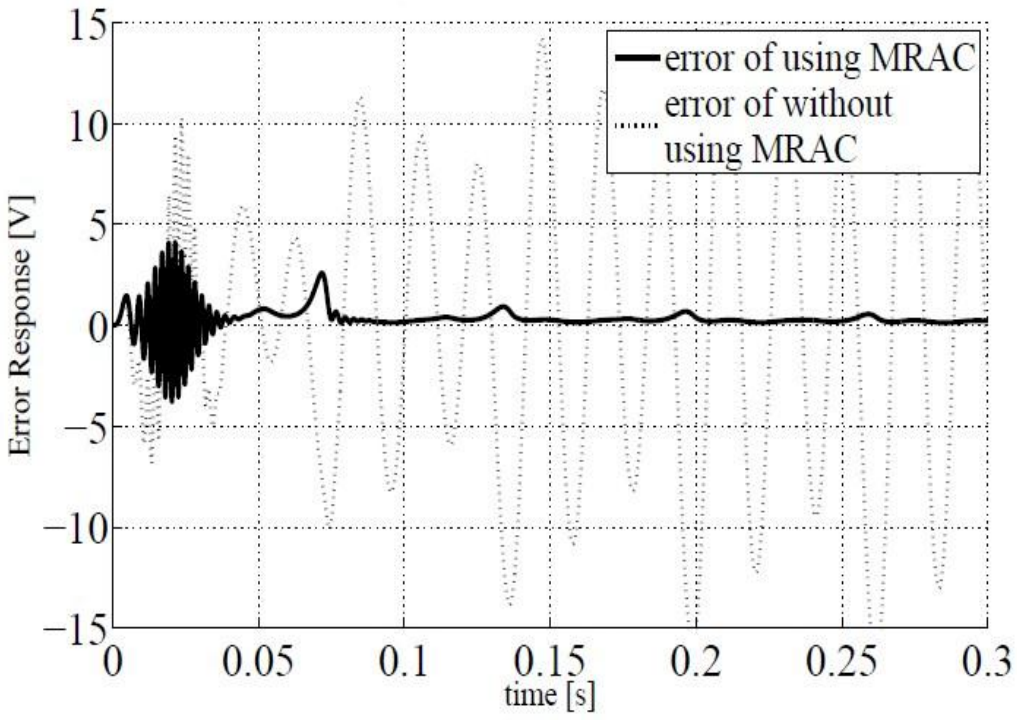

Figure 17: The error comparison of the sinusoidal input.

Last but not the least; it is instructive to know that one essential assumption in designing this MRAC controller is this MRAC design is independent of the external perturbance consideration. One reason is that it is hard to measure and model the noise or disturbance of the photovoltaic power conversion system in the experiment with so many constrains. In additional, assuming the model of perturbance is known, it will significantly make the MRAC system complex enough to maintain the robust performance of the MRAC control design and it will be overwhelming in the realization. The second reason is that under the condition of modeling perturbance source, the photovoltaic system's convergence performance with those obtained adaptive laws will not be asymptotically stable in the sense of Lyapunov. Therefore, the future work in the MRAC designing improvement will mainly mitigate the effect of perturbance in the system.

Given those simulation results obtained above, several conclusions about the MRAC algorithm could be drawn. Firstly, the convergence rate of MRAC system could be obtained extremely fast, being within one second, which is trivial enough to be noticed in the real application. Secondly, no matter how the solar insolation and temperature changes, in term of the plant description: the constantly changing damping ratio of the transfer function, MRAC algorithm is always capable of tuning the plant model within a very short time, regardless of the value of resistor. Having proven the stability and robustness of the MRAC algorithm from the series of straightforward illustrations, another proof is tested to compare the controller parameter from the actual simulation and the ideally calculation. By comparing the nominal controller parameter and the practical controller parameter, it can mathematically prove the asymptotically convergence is valid. The comparison between the nominal controller's parameters and the updated controller's parameters is shown in Table 2. As shown in the table, a reasonable agreement is obtained thereby demonstrating that the controller will

converge to the optimal power point. Based on the assumption of the plant that N_{p} is monic Hurwitz polynomial, the transfer function of the plant, after adaption, will still be a second-order system. This is because the zero-pole cancellation takes place within the open left-hand side of the s-plane.

Table 2: Comparison between the nominal and actual controller parameters

	θ_1	θ_2	θ_3	c_0
Nominal controller parameters for plant I	-5.8	6.315	-0.515	1
Updated controller parameters for plant I	-5.8	6.287	-0.500	1
Nominal controller parameters for plant II	-5.94	6.56	-0.6204	1
Updated controller parameters for plant II	-5.94	6.04	-0.6239	1

5.0 CONCLUSION AND FUTURE WORK

In order to improve the efficiency of photovoltaic systems, MPPT control algorithms are used to optimize the power output of the systems. The essential considerations are the accuracy and convergence time. As the simulation result extensively discussed in Section 4, the statement that the proposed control system, by coupling two control algorithms, optimizes the performance of the solution to the maximum power point tracking is convincing. As reported in the literature, the duty cycle is obtained faster through the RCC method, which is in the unit of millisecond. In the MRAC control system, the time constant of converging to the characteristic of the reference model is couple of seconds and it is longer, compared to the time constant of RCC. By tuning the adaptive gain in the adaptive law, the time constant can be modulated to guarantee the stability of the entire system. By simulating the system through different types of inputs, the proposed control system is sufficient robust and stable to endure the small perturbance in the input and the measurements.

In the future work, related optimization work for this control system is mainly on two aspects. Firstly, the RCC algorithm can be improved from the view of simple implementation. As reported in the literature, the control law is not reliable enough to sustain the perturbance of the noise. Proposing an alternative control law is plausible. Secondly, the MRAC algorithm can be further well-designed with the consideration of the model of perturbance, so that the performance of the MRAC can be enough robust. Thirdly, by implementing the RCC algorithm in the simulation environment or the actual hardware

realization, the entire proposed control system can be simulated to test the performance of the system.

APPENDIX A

MRAC CODING IN THE SIMULATION

```
function [ ky1h,ky2h,krh] = mrac( input,refnum,refden,ky1,ky2,kr )

ky1hat=10;
ky2hat=10;
kr=10;
bm=refnum(1,1);
am1=refden(1,2);
am2=refden(1,3);
ap1=-(ky1hat+ky2hat);
ap2=ky1hat*ky2hat;
bp=(ap2*bm)/(am2);
plantnum=[bp];
plantden=[1,am1,am2];
t=[0:0.1:10];
r=10;

for j=1:10
yp=step(plantnum,plantden,t);
ym=step(refnum,refden,t);
dyp=yp(2:length(yp))-yp(1:length(yp)-1);
dym=ym(2:length(ym))-ym(1:length(ym)-1);
temp1=(dyp-dym).*(dyp);
temp2=(dyp-dym).*(yp(1:length(yp)));
temp3=(dyp-dym)*(input).*(t(1:length(t)-1));
ky1h=-r*(bp)*(sum(temp1));
ky2h=-r*(bp)*(sum(temp2));
krh=-r*(bp)*(sum(temp3));
resulttemp=[ky1h,ky2h,krh];

end

end
```

APPENDIX B

DATA COMPARISON CODING

```
function mraccompfirst

load('error');
load('error1');
load('plantwithmrac');
load('reference');
load('plantwithoutmrac');
ref=referencemodel(2,:);
plantwithmrac=pwith(2,:);
plantwithoutmrac=pwithout(2,:);
errortwo=error1(2,:);
t=[40/400001:40/400001:40];
errorone=error(2,:);
figure;
hold on;

%plot(t,errorone);
%plot(t,errortwo);
plot(t,plantwithmrac);
plot(t,plantwithoutmrac);
plot(t,ref);
grid on;
xlabel('time(s)');
ylabel('the error');
```

BIBLIOGRAPHY

[1]. Femia, N., et al., *Optimization of perturb and observe maximum power point tracking method.* Power Electronics, IEEE Transactions on, 2005. **20**(4): p. 963-973.

[2]. Brunton, S.L., et al., *Maximum power point tracking for photovoltaic optimization using ripple-based extremum seeking control.* Power Electronics, IEEE Transactions on, 2010. **25**(10): p. 2531-2540.

[3]. Esram, T., et al., *Dynamic maximum power point tracking of photovoltaic arrays using ripple correlation control.* Power Electronics, IEEE Transactions on, 2006. **21**(5): p. 1282-1291.

[4]. Abdelsalam, A.K., et al., *High-performance adaptive perturb and observe MPPT technique for photovoltaic-based microgrids.* Power Electronics, IEEE Transactions on, 2011. **26**(4): p. 1010-1021.

[5]. Masoum, M.A.S., H. Dehbonei, and E.F. Fuchs, *Theoretical and experimental analyses of photovoltaic systems with voltageand current-based maximum power-point tracking.* Energy conversion, IEEE transactions on, 2002. **17**(4): p. 514-522.

[6]. Esram, T. and P.L. Chapman, *Comparison of photovoltaic array maximum power point tracking techniques.* Energy conversion, IEEE transactions on, 2007. **22**(2): p. 439-449.

[7]. Veerachary, M., T. Senjyu, and K. Uezato, *Neural-network-based maximum-power-point tracking of coupled-inductor interleaved-boost-converter-supplied PV system using fuzzy controller.* Industrial Electronics, IEEE Transactions on, 2003. **50**(4): p. 749-758.

[8]. Kimball, J.W. and P.T. Krein, *Discrete-time ripple correlation control for maximum power point tracking.* Power Electronics, IEEE Transactions on, 2008. **23**(5): p. 2353-2362.

[9]. Krein, P.T. *Ripple correlation control, with some applications*. in *Circuits and Systems, 1999. ISCAS'99. Proceedings of the 1999 IEEE International Symposium on*. 1999. IEEE.

[10]. Logue, D. and P. Krein. *Optimization of power electronic systems using ripple correlation control: a dynamic programming approach*. in *Power Electronics Specialists Conference, 2001. PESC. 2001 IEEE 32nd Annual*. 2001. IEEE.

[11]. Ioannou, P.A., *Adaptive systems with reduced models.* Lecture Notes in Control and Information Sciences, 1983.

[12]. Miller, D.E., *A new approach to model reference adaptive control.* Automatic Control, IEEE Transactions on, 2003. **48**(5): p. 743-757.

[13]. Narendra, K. and L. Valavani, *Stable adaptive controller design--Direct control.* Automatic Control, IEEE Transactions on, 1978. **23**(4): p. 570-583.

[14]. Narendra, K.S. and A.M. Annaswamy, *Stable adaptive systems*. 2005: Dover Publications.

[15]. Narendra, K.S. and P. Kudva, *Stable adaptive schemes for system identification and control-part I.* Systems, Man and Cybernetics, IEEE Transactions on, 1974(6): p. 542-551.

[16]. Sastry, S. and M. Bodson, *Adaptive control: stability, convergence and robustness*. 2011: Dover Publications.

[17]. Solodovnik, E.V., S. Liu, and R.A. Dougal, *Power controller design for maximum power tracking in solar installations.* Power Electronics, IEEE Transactions on, 2004. **19**(5): p. 1295-1304.

[18]. Jain, S. and V. Agarwal, *A new algorithm for rapid tracking of approximate maximum power point in photovoltaic systems.* Power Electronics Letters, IEEE, 2004. **2**(1): p. 16-19.